Star formation newsletter

大橋聡史

First detection of CF+ towards a high-mass protostar

Fechtenbaum et al. A&A

大質量(44Msun)class 0のコアからCF+(C+のトレーサー)が検出

PDRが近くにないので、accretion shock(X-ray)かoutflowによってC+が生成

まだUCHIIになる前から電離した領域が存在している

→hot coreのchemical evolutionを考える上で、非常に若い段階から電離されていることが判明

$$F + H_2 \rightarrow HF + H \qquad \text{and} \qquad HF + C^+ \rightarrow CF^+ + H,$$

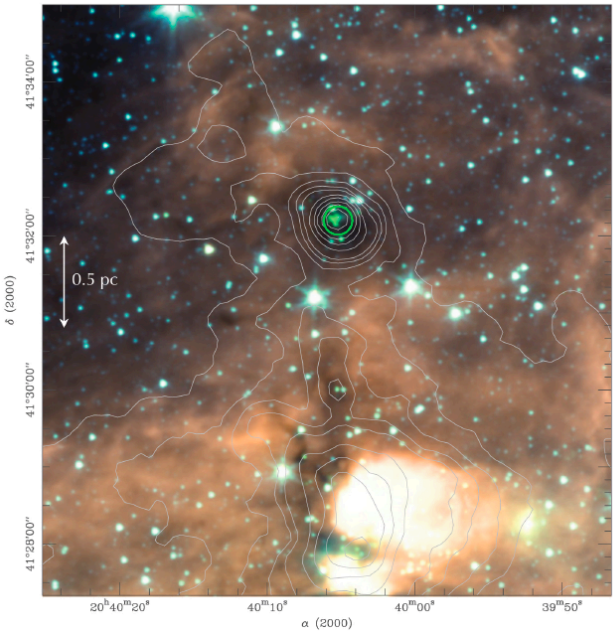

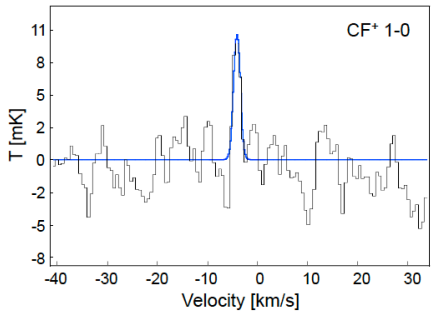

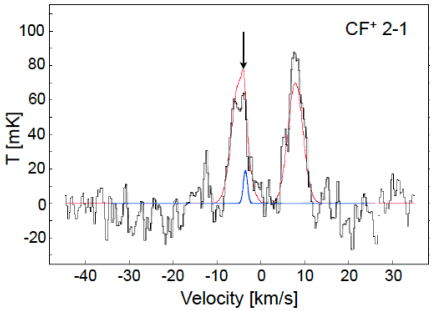

←CH3OHとのコンタミ

The density structure and star formation rate of non-isothermal polytropic turbulence

Christoph Federrath & Supratik Banerjee accepted in MNRAS

ISMはスケールによって乱流や磁場だけでなく比熱も異なる。isothermalの計算が主流だが、今回はpolytropicでΓ=0.7, 1.0, 5/3で計算

$$P \sim \rho^{\Gamma}, T \sim \rho^{\Gamma-1}$$

Γ<1以下で分裂しやすく、Γ>1でsmooth

PDFも変化、density variation-Mach number関係にΓの関数を新たに発見

new PDFを用いたSFRは0.7から5/3で5倍ほど変化する

密度

温度

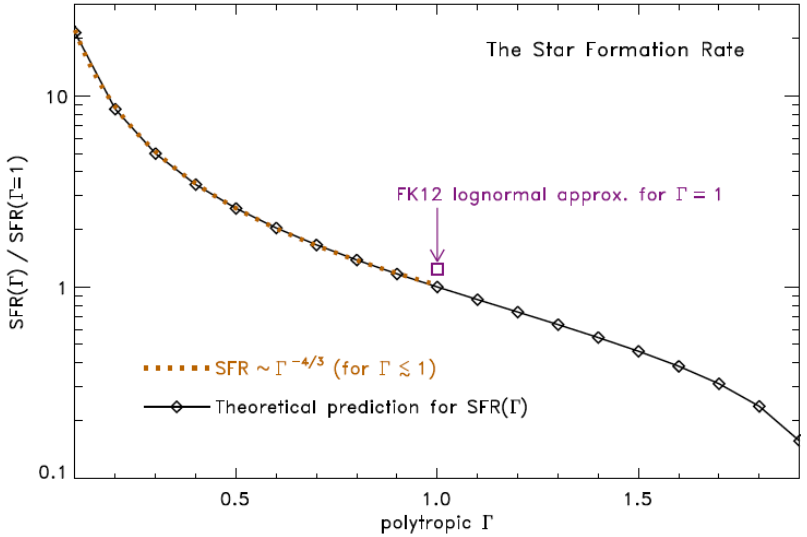

$$\mathrm{SFR} \sim \frac{1}{2}\exp\left(\frac{3}{8}\sigma_{s,V}^2\right)\left[1+\mathrm{erf}\left(\frac{\sigma_{s,V}^2 - s_{\mathrm{crit}}}{\left(2\sigma_{s,V}^2\right)^{1/2}}\right)\right].$$

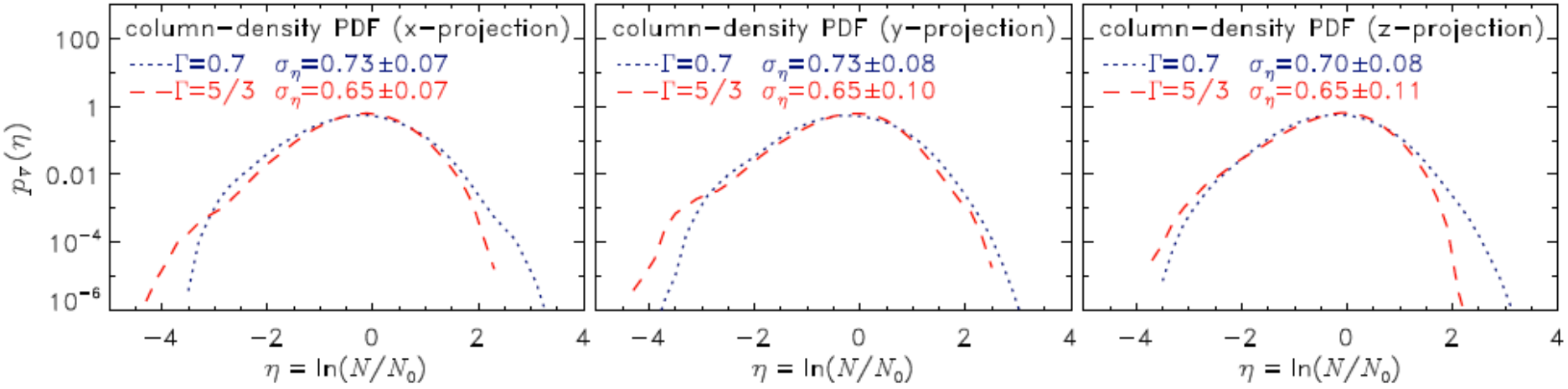

Spectroscopic characterization of X-ray emitting young stars associated with the Sh 2-296 nebula

B. Fernandes et al. accepted in MNRAS

反射星雲(Cma R1)にあるX線星をopticalによるHα, リチウム線で調べた

Geminiで

41/58がT-tauri, 15はとても若い原始星

T-tauriのうち17%が古典的、83%は弱輝線Tタウリ星

が、これらは質量や年齢に違いはなかった

近赤から中間赤外での観測では半分ほどが1-2Myrの若い星だったが、25%しかIR超過が見られず、他の領域と比べて円盤保有率が少ない

→external factorがdick散逸を加速させているのでは

観測

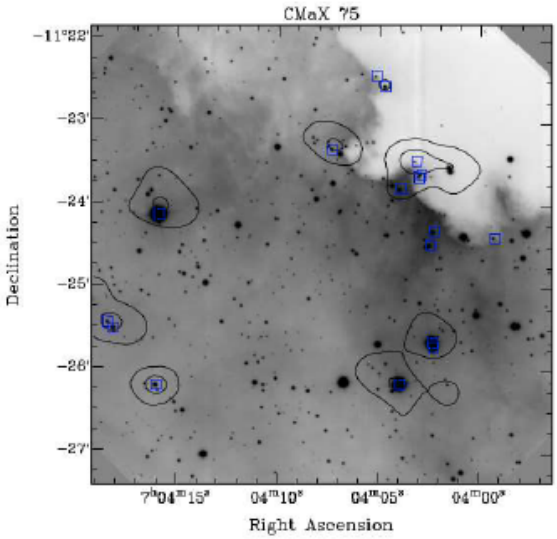

SED フィット

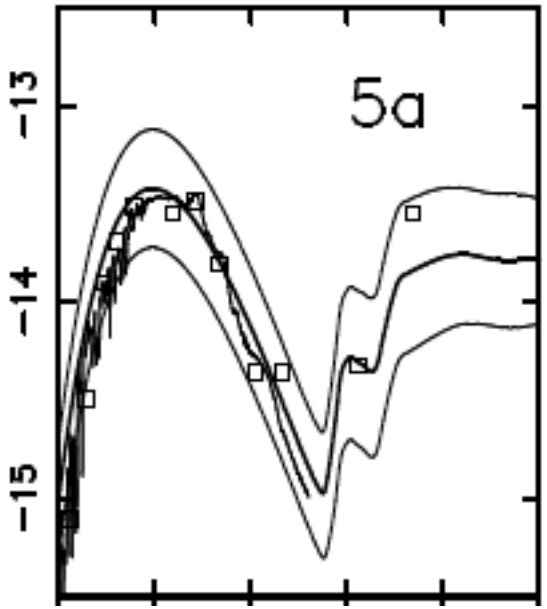

スペクトル

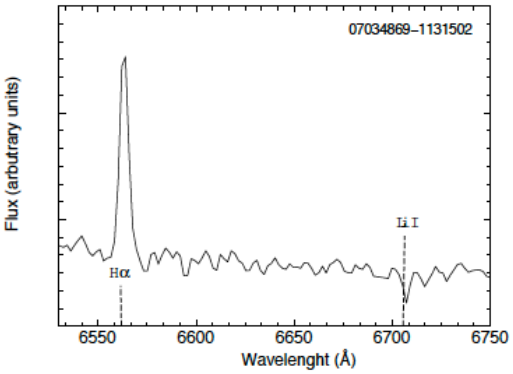

CTTとWTTに違いはあまりない

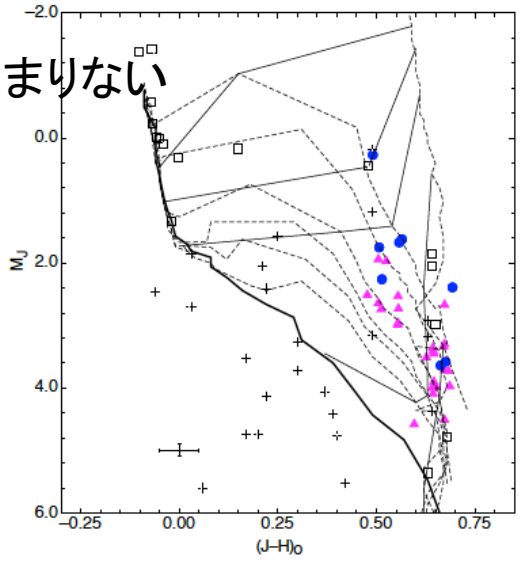

Figure 8. Near-IR colour-magnitude diagram for stars in our sample. CTTs and WTTs are respectively represented by filled circles and triangles. Open squares show the PMS star candidates and crosses indicate the remaining unclassified stars. Isochrones with ages of 0.1, 1, 2, 5, 8, 10 and 15 Myr (dashed lines) and the ZAMS (thick line) from Siess et al. (2000). The thin lines represent the tracks for masses of 0.2, 1, 2, 3 and 4 $M_\odot$.

分類

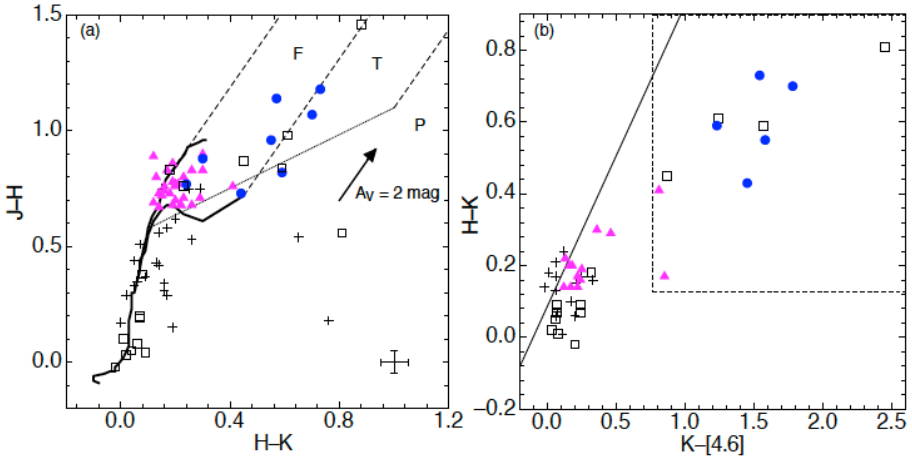

Optical and infrared counterparts of the X-ray sources detected in the Chandra Cygnus OB2 Legacy Survey

Guarcello et al. in ApJ

Cygnus OB2領域でのX線でカタログした天体を光赤外とコンバイン
マッチングプロシジャーと5703天体のカタログ化

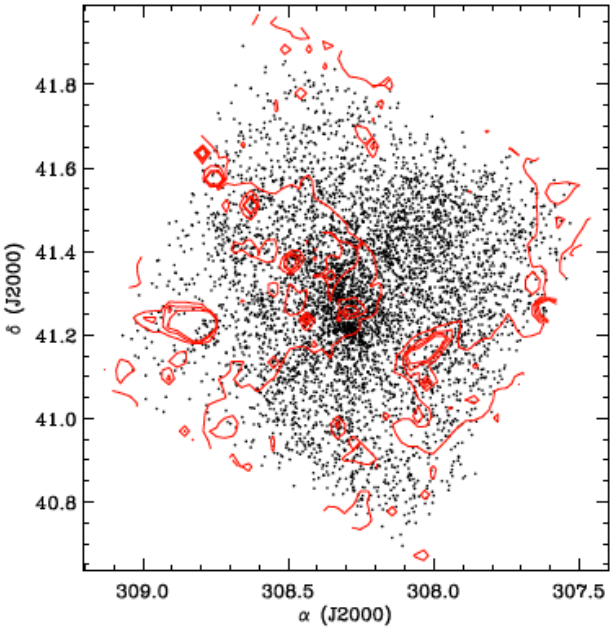

Fig. 9.— Spatial distribution of the X-ray sources with reliable OIR counterparts. The red solid lines mark the emission contours at 8.0 μm.

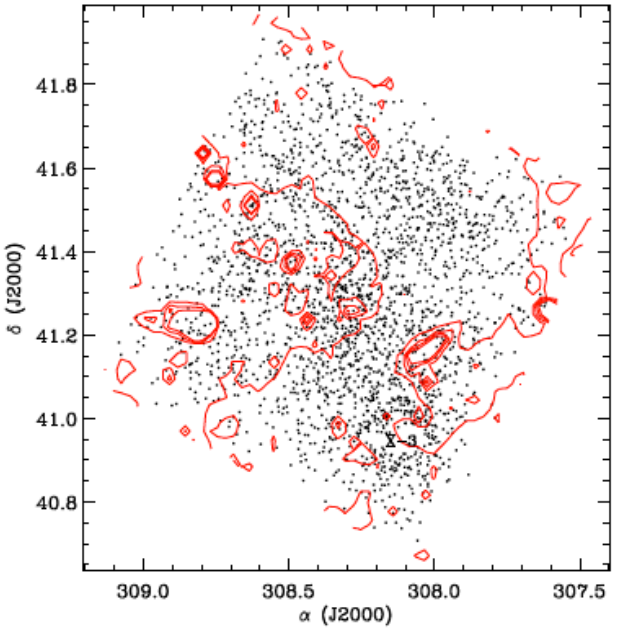

Fig. 10.— Spatial distribution of the X-ray sources without OIR counterparts, with over-plotted the emission contours at 8.0 μm.

Structure and Stability of Filamentary Clouds Supported by Lateral Magnetic Field

Hanawa & Tomisaka in ApJ

難しい…

磁場に支えられたコアの安定性を調べた（thin diskと近似できる）

磁場なしの線質量

$$\lambda \equiv \int_0^\infty 2\pi r\rho(r)dr = \frac{2c_s^2}{G},$$

磁場ありの線質量

$$\lambda = \frac{c_s^2}{2G} + \sqrt{\left(\frac{\Phi}{2\pi\sqrt{G}}\right)^2 + \left(\frac{c_s^2}{2G}\right)^2},$$

臨界質量磁束比

$$M/\Phi = (2\pi\sqrt{G})^{-1}$$

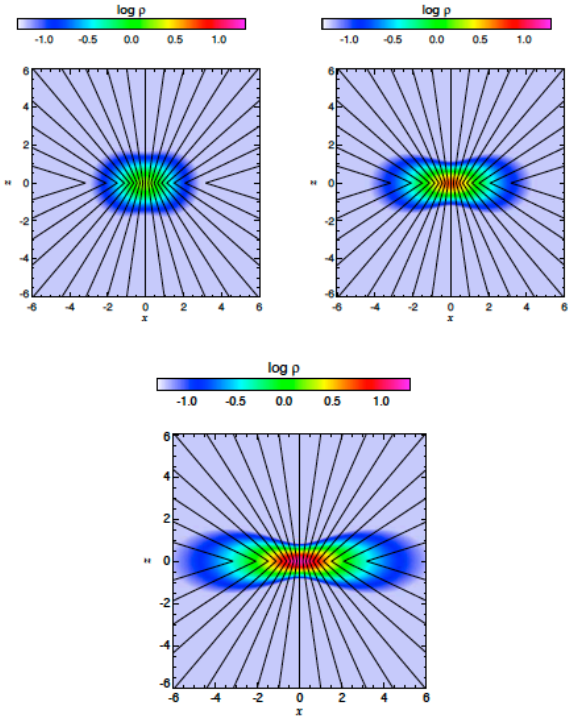

Fig. 1.— The cross sections show the density by color and the magnetic field by lines. The upper left and right panels are for $\lambda = 5$ and $10c_s^2/G$, respectively. The bottom one is for $\lambda = 20c_s^2/G$.

Structure and Stability of Filamentary Clouds Supported by Lateral Magnetic Field

Hanawa & Tomisaka in ApJ

フィラメントと垂直な磁場では
臨界質量磁束比以下では安定,
表面密度や密度が非常に高い場合のみ
不安定になる

臨界値

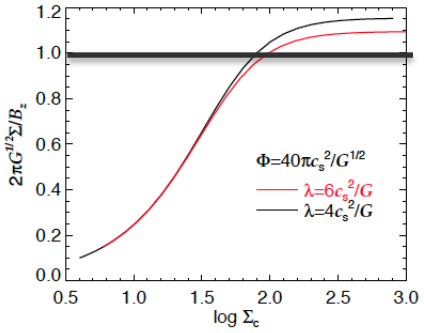

Fig. 4.— The mass to flux ratio at the cloud center is shown as a function of the surface density at the cloud center for given λ and Φ, which are taken to be $\lambda = 4c_s^2/G$ and $\Phi = 8\pi c_s^2/\sqrt{G}$ for the black curve and $\lambda = 6c_s^2/G$ and $\Phi = 8\pi c_s^2/\sqrt{G}$ for the red curve,

臨界値

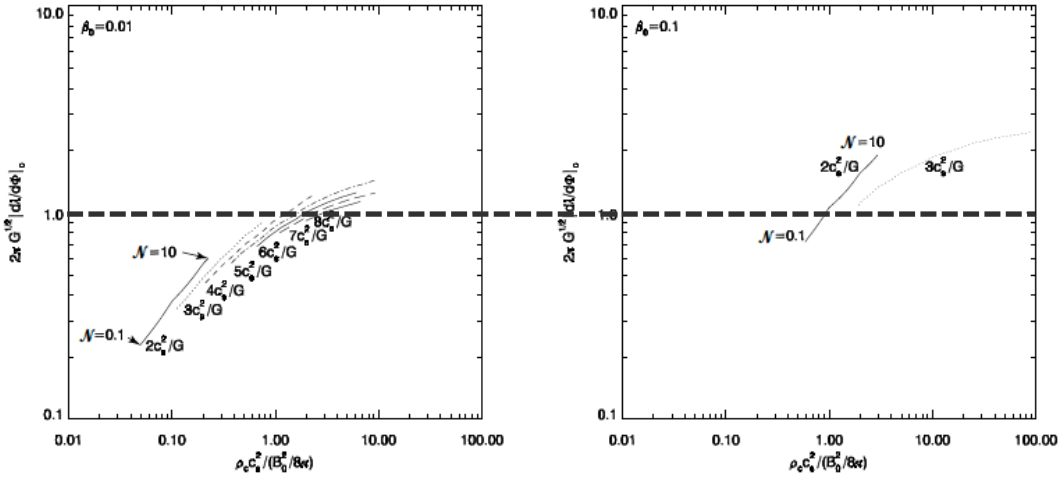

Fig. 5.— The mass to flux ratio at the cloud center is shown as a function of the density thereof in 2D models. The curves denote the loci of constant λ of which values are labelled. The central density is denoted in unit of $B_0^2/8\pi c_s^2$. The index, $\mathcal{N}$, increases from left to right along the loci. The left and right panels denote the models of $\beta_0 = 0.01$ and 0.1, respectively.